Martí Calatayud, MC.; Evdochenko, E.; Bär, J.; García Gabaldón, M.; Wessling, M.; Pérez-Herranz, V. (2020). Tracking homogeneous reactions during electrodialysis of organic acids via EIS. Journal of Membrane Science. 595:1-10. https://doi.org/10.1016/j.memsci.2019.117592

Tracking homogeneous reactions during electrodialysis of organic acids via EIS

M.C. Martí-Calatayud[a,*], E. Evdochenko[b], J. Bär[b], M. García-Gabaldón[a], M. Wessling[b,c], V. Pérez-Herranz[a]

[a] *Universitat Politècnica de València, IEC Group, Departament d'Enginyeria Quimica i Nuclear, Camí de Vera s/n, 46022, València, Spain*
[b] *RWTH Aachen University, Chemical Process Engineering, Forckenbeckstr. 51, 52074 Aachen, Germany*
[c] *DWI Interactive Materials Research, Forckenbeckstr. 50, 52074 Aachen, Germany*

Abstract

Organic acids are highly valuable platform chemicals that can be obtained from bioresources and subsequently transformed into a wide spectrum of profitable consumer goods. After their synthesis, organic acids need to be separated from other by-products and conveniently upconcentrated. Based on the ionic nature of organic acids, electromembrane processes are viable technologies for their recovery. Transport of weak acids through ion-exchange membranes is a complex process influenced by multiple phenomena, i.e. concentration polarization, water dissociation and counterion-membrane interactions. In the present study, the transport of two different organic acids (citric and oxalic acid) through anion-exchange membranes is investigated by means of using linear sweep voltammetry, chronopotentiometry and electrochemical impedance spectroscopy (EIS). Results have shown that, at pH

*I am corresponding author
Email addresses: mcmarti@iqn.upv.es (M.C. Martí-Calatayud), manuscripts.cvt@avt.rwth-aachen.de (M. Wessling), vperez@iqn.upv.es (V. Pérez-Herranz)

values where multivalent acid anions predominate in solution, a first limiting current density is registered in the current-voltage curves, followed by an increase in membrane resistance. A further increase in current leads to a second limiting current density and a steeper increase in membrane resistance associated with an intensified ion depletion. A strong correlation between polarization curves and electrochemical impedance measurements reveals that such increase in resistance is prompted by generation of H^+ and OH^- ions and the concomitant onset of homogeneous reactions in very thin solution layers. The generation of H^+ and OH^- ions is tracked by a Gerischer arc in the impedance spectra. As the polarization level increases, the subsequent reaction of multivalent anions into lower-charge acid anions involves the evolution of additional Gerischer arcs. Furthermore, the lower conductivity of the reaction products correlates with the increased system resistance. The characteristic times of these reactions are in the order of milliseconds, thus being only directly accessible with the use of frequency response analysis techniques, such as EIS.

Keywords: electrodialysis, weak electrolytes, electrochemical impedance spectroscopy (EIS), platform chemicals, organic acid recovery, biorefinery

---

Nomenclature

Abbreviations

AC	Alternate Current
EIS	Electrochemical Impedance Spectroscopy
BMED	Bipolar Membrane Electrodialysis
DC	Direct Current

ED	Electrodialysis
LSV	Linear Sweep Voltammetry

Symbols

ω	Angular frequency
φ	Phase shift between voltage and current signals
$I(t)$	Current as a function of time
I_0	Amplitude of the AC component of the current signal
I_{DC}	DC component of the current signal
i_{lim1}	First limiting current density
i_{lim2}	Second limiting current density
i_{lim}	Limiting current density
$Im(Z)$	Imaginary part of the electrochemical impedance
j	Imaginary unit
$Re(Z)$	Real part of the electrochemical impedance
$U(t)$	Voltage as a function of time
U_0	Amplitude of the AC component of the voltage signal
U_{DC}	DC component of the voltage signal
Z	Electrochemical Impedance

1. Introduction

Sustainable production of specialty chemicals has become an imperative need in modern societies, considering the environmental issues associated with the use of fossil resources as primary source for fuels and daily-use products. Platform chemicals constitute building blocks that are intermediates in the synthesis pathway from raw bio-based materials to final products. They

are used for the synthesis of engineering plastics, food additives, health-care goods or pharmaceuticals, among others. Despite the notable achievements attained in the fabrication of bio-based products, separation and purification of platform chemicals still pose a prominent limitation in the development of cost-efficient biorefineries [1, 2].

Organic acids are an important class of platform chemicals, which can be produced via diverse routes, i.e. catalytic cleavage of biomass, lignin depolymerization or carbohydrate fermentation [3–8]. They form electrolytes in aqueous solutions, giving rise to ionic compounds. Consequently, electromembrane processes, such as electrodialysis (ED), bipolar membrane electrodialysis (BMED)or electrodeionization, have been used for their separation and upconcentration [9–11]. Electromembrane processes are based on the selective permeation of ions through ion-exchangemembranes driven by an electric field. Cation- and anion-exchange membranes are arranged in an alternating fashion to produce concentrated and diluted streams. These processes are recognized as proper technologies for biorefinery production schemes, since they can be coupled with fermentation reactors, imply minimal addition of reagents, can be easily scaled up and powered by renewable sources of energy [12–14].

Transport of organic acids through ion-exchange membranes has been the subject of study of many researches. Most studies are based on batch electrodialysis experiments focusing on optimization of membrane configuration, current density regime or solution pH. A. Chandra et al. determined

the potential, flow rate and feed concentration that maximized current efficiency during the electrodialytic recovery of citric acid [15]. S. J. Andersen et al. investigated the extraction of short-chain carboxylates from fermentation broths by means of ED coupled with subsequent biphasic esterification [16]. Commonly, sudden drops in current efficiency, jumps in voltage drop or degradation of the membranes are reported during the course of the experiments [17–20]. On this subject, a fundamental understanding of the complex events occurring during the recovery of organic acids by ED is lacking.

One of the most relevant phenomena that govern ion transport in electromembrane processes is concentration polarization. As a consequence of membrane selectivity, transport number of counterions through ion-exchange membranes is higher than within the neighboring solution layers.This difference results in the formation of diffusion boundary layers: the concentration of ions in the diluate side next to the membrane decreases, while it increases at the concentrate side. At low polarization levels (low transmembrane voltages), the behavior of the system can be assumed to be quasi-ohmic and the decrease in conductivity at the diluate side is compensated by the increase taking place at the concentrate side. However, as the level of polarization is increased, the concentration gradients at both sides of the membrane become more pronounced. A limit is reached when the concentration at the diluate membrane-solution interface approaches zero: the so-called limiting current density (i_{lim}) is reached and the resistance of the system grows considerably. At this point, a further increase in the driving force does not induce a rise in current density, at least until additional mass transfer phenomena supplying

ions to the membrane are induced. When the membrane voltage drop exceeds a certain threshold, overlimiting mass transfer mechanisms such as electroconvection and water dissociation can come into play. Electroconvection results in the formation of chaotic vortices in the diluted diffusion boundary layer that bring counterions from the bulk towards the membrane surface. Differently, the dissociation of water molecules takes place right at the membrane interface. Both phenomena culminate in an increase in current density beyond the plateau region, leading to the third part of current-voltage curves. In ED of strong electrolytes, electroconvection is usually preferred, since the increase in current is mainly carried by the target solution counterions. However, the development of concentration polarization in weak electrolytes is a more complex process, owing to the presence of multiple counterions, which can participate in equilibrium reactions with the products of water dissociation.

The treatment commonly adopted for ED of strong electrolytes, a well-established process, cannot be extrapolated by default for ED of organic acids. Contrary to strong electrolytes, where salts are fully dissociated in their forming ions, organic acids are weak electrolytes and only dissociate partially into their respective anions and cations. Mainly solution pH, but also total electrolyte concentration or presence of coions determine the electrolyte speciation and, in turn, the type and amount of current carriers. Extensive investigations about transport of weak electrolytes of inorganic nature has shown that shifts in the equilibrium are concomitant to variations in the level of applied current density [21–25]. Most importantly, such

changes may imply a variation in the resistance of membrane systems, which are manifested in the form of atypical current-voltage curves [24, 25]. In this vein, Melnikova et al. identified two plateau regions relating to two different limiting current densities, and attributed the first limiting current to the depletion of ions at the membrane surface [26]. Above the first limiting current, acid anions dissociated as they entered the membrane, releasing H^+ ions at the depleted membrane/solution interface and OH^- ions at the concentrate membrane/solution interface. The resulting H^+ and OH^- ions, caused a rise in current density, until the membrane was almost completely converted into the multivalent anion form. Rybalkina et al. reported similar effects with phosphoric acid anions [27].The peculiar current-voltage curves obtained for organic acids have been likewise reproduced in 1-dimensional mechanistic simulations [28]. In this regard, it is important to take into account two trends observed in the literature, which are of special relevance for the present investigation. First, it has been widely confirmed that anion-exchange membranes are more prone to induce catalytic water dissociation-than cation-exchange ones [29–31]. Second, the dissociation of water at high current densities hampers the progress of electroconvection, because the generated H^+ and OH^- ions access the space charge region developed at the membrane-solution interface [32–34].

Current efficiency and membrane voltage drops are key indicatorsof the yield and energy consumption of electromembrane processes, respectively. Systematic analysis by means of sound and precise techniques is therefore necessary to give insight into the mass transfer phenomena involved during

the transport of organic acids through ion-exchange membranes at different current densities. Getting a better understanding on the interplay between the involved factors and controlling the performance of ED of weak electrolytes is a central milestone in the design of optimum downstream processing of organic acids. In the present work, the current-voltage relationship describing the migration of organic anions through permselective membranes is studied in depth via Electrochemical Impedance Spectroscopy (EIS). EIS is a frequency response analysis technique applicable to decomposing the resistance of electrochemical systems into several contributions, each of them being associated with mass transfer phenomena showing up at different characteristic times.

2. Experimental

2.1. Electrolytes and membranes

Two organic acids with different number of carbon atoms and carboxylic groups have been selected for the present investigation: citric acid and oxalic acid. Solutions from the acid and sodium salt forms of both were prepared from the following reagents: $H_2C_2O_4 \cdot 2\,H_2O$, $Na_2C_2O_4$, $C_6H_8O_7$ and $C_6H_5Na_3O_7 \cdot 2\,H_2O$, all supplied by Panreac Química SLU (Spain). For the sake of readability, the anion of citric acid, citrate ($C_6H_5O_7^{3-}$), will be referred to as Cit^{3-} in this work. Analogously, the oxalate anion ($C_2O_4^{2-}$) will be referred to as Ox^{2-}. Both organic acids exhibit the attributes of weak electrolytes: they do not dissociate completely in aqueous solutions into their respective anions and cations. Citric acid is a triprotic acid that can undergo

successive deprotonation reactions, as shown below:

$$H_3Cit \rightleftharpoons H_2Cit^- + H^+ \quad (1)$$

$$H_2Cit^- \rightleftharpoons HCit^{2-} + H^+ \quad (2)$$

$$HCit^{2-} \rightleftharpoons Cit^{3-} + H^+ \quad (3)$$

with pKa_1, pKa_2 and pKa_3 values of 3.128, 4.761 and 6.396, respectively (25 °C). Furthermore, Cit^{3-}ions may combine with Na^+ ions according to:

$$Cit^{3-} + Na^+ \rightleftharpoons NaCit^{2-} \quad (4)$$

where $logK = 1.4$.

Oxalic acid is a dicarboxylic acid, which can lose up to two protons:

$$H_2Ox \rightleftharpoons HOx^- + H^+ \quad (5)$$

$$HOx^- \rightleftharpoons Ox^{2-} + H^+ \quad (6)$$

The pKa_1 and pKa_2 values corresponding to reactions 5 and 6 are 1.252 and 4.266, respectively [35]. Oxalate anions can also recombine with Na^+ according to the following equilibrium:

$$Ox^{2-} + Na^+ \rightleftharpoons NaOx^- \quad (7)$$

where $logK = 0.9$.

The equilibrium diagrams of the H_3Cit/Na_3Cit and H_2Ox/Na_2Ox systems

are plotted in Fig. 1 for a wide range of pH values. The undissociated acid forms predominate at very low pH values, while the formation of multiply charged anions is favored at increasing pH values. Moreover, here it is to be noted that, in the membrane phase, the presence of complex species of $NaOx^{-}$ is less likely to occur than in solution because of the exclusion of Na^{+} ions by the membrane fixed charges.In order to investigate the effect of the predominating species on ion transport through the membranes, different mixtures of the acids and their corresponding salts were prepared in distilled water at a total concentration of either Cit^{3-}or Ox^{2-}species of 0.05 M. The dashed vertical lines in the speciation diagrams indicate the pH of the working solutions prepared. Depending on the method used to obtain organic acids from biomass, the ED feed solutions coming from previous fermentation broths can cover a wide pH spectrum [9, 15, 36, 37]. In addition to organic acid solutions, electrochemical measurements were also conducted with 0.05 M NaCl solutions, and were taken as a reference of a strong electrolyte for comparison purposes.

The limiting step during the recovery of organic acids is the transport of the acid anions through anion-exchange membranes. Consequently, this will be the main subject of study in the present work. Commercial anion-exchange membranes HDX200 (Ionsep-HC-A, supplied by Hidrodex) were used for this investigation. These membranes have a heterogeneous structure with reinforcing fabrics and have a concentration of 1.8 meq of quaternary amine groups per gram of membrane. The diluate compartments of the ED experimental setup is separated from the cathode by HDX100 cation-

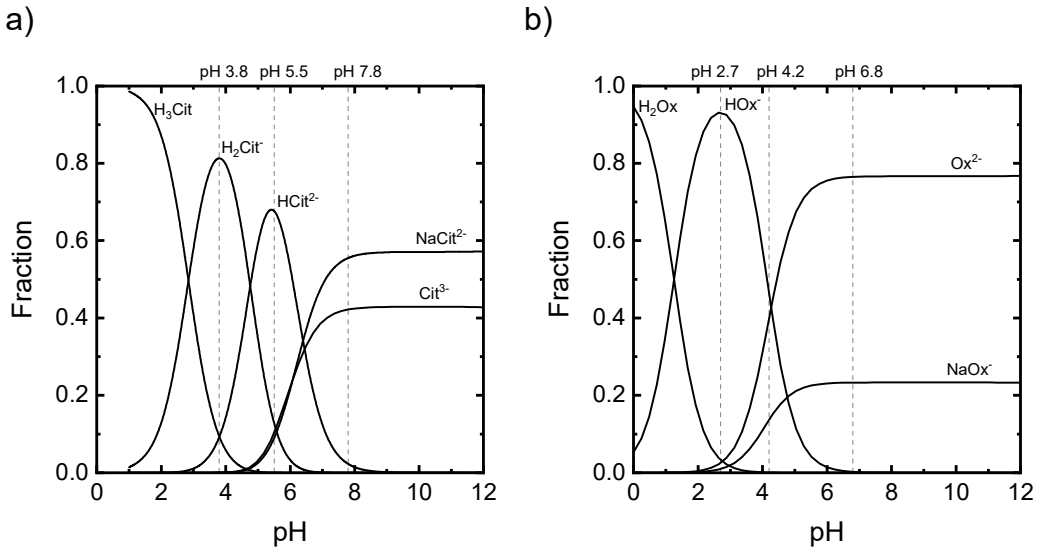

Figure 1: Speciation diagrams for (a) 0.05 M H_3Cit/Na_3Cit solutions and (b) 0.05 M H_2Ox/Na_2Ox solutions.

Table 1: Properties of the ion-exchange membranes used in the present work.

ion-exchange membrane	fixed charged group	ion-exchange capacity (meq/gr)	thickness (mm)	water uptake
IONSEP-HC-A	quaternary amine	1.8	0.42	40%
IONSEP-HC-C	sulfonic acid	2.0	0.42	40%

exchange membranes (Ionsep-HC-C). The properties of both membranes are summarized in 1.

2.2. Experimental setup for the electrochemical measurements

The electrochemical measurements performed in this work were conducted using a four electrode configuration. The setup consisted of three compartments, each one with 130 mL volume capacity, separated by ion exchange membranes, which is described in detail in previous publications [38, 23]. The

anion-exchange membrane had an effective membrane area of 1 cm^2 and was equilibrated with the electrolyte solution overnight prior to the experiments. Voltage was recorded between a pair of Ag/AgCl reference electrodes. These were immersed in luggin capillaries, installed at both sides of the membrane under study. The working and counter electrodes consisted of two graphite bars placed at the anodic and cathodic compartments, respectively. The three compartments were completely filled with the measuring solution and experiments were conducted at room temperature. All electrochemical measurements were performed using a potentiostat/galvanostat from Metrohm, model Autolab PGSTAT302N. Results were sampled and treated with the software Nova v. 2.1.

2.3. Current-voltage behavior

Linear sweep voltammetry (LSV) and chronopotentiometry were conducted to obtain the current-voltage behavior of the membrane-electrolyte systems. LSV measurements were applied by increasing the potential up to 3 V at a scan rate of 5 mV/s. Meanwhile, the resulting current was sampled. Subsequently, we identified characteristic regions of the polarization curves and conducted various chronopotentiometric measurements in each of them. For every investigated point of the curves, a constant current was applied for 300 s and the resulting potential drop was recorded. Afterward, the current was set to zero and the relaxation phase was recorded for 100 s before moving on to the next measurement point.

2.4. Impedance measurements

Further analysis at selected working points corresponding to different regions of the polarization curves were performed through EIS. A sinusoidal voltage was imposed to the system over a given voltage bias. The frequency range of the impedance experiments was 10^5 Hz to 2.5 mHz and the voltage amplitude was 10 mV. The amplitude was chosen to be high enough to minimize noise effects and small enough to comprise a range of linear current-voltage behavior. High frequencies (until 10 Hz) were measured at least three times to improve accuracy, while the measurement time at frequencies smaller than 50 mHz was increased to 100 s.

The input voltage signal imposed to the system takes the following form:

$$U(t) = U_{DC} + U_0 \cdot sin(\omega t) \tag{8}$$

where $U(t)$ represents the total voltage, U_{DC} is the DC component, and U_0 and ω stand for the amplitude of the AC component and the angular frequency, respectively. When U_0 is small enough, the behavior of the system is linear and the electric current through the system will respond with a sinusoidal function with the same frequency, but displaced in time:

$$I(t) = I_{DC} + I_0 \cdot sin(\omega t + \varphi) \tag{9}$$

where I_{DC}, I_0 and φ represent the DC component of the current signal, the amplitude of the AC component of current and the phase shift between $U(t)$ and $I(t)$ signals. The impedance of the system, Z, is given by the following

equation:

$$Z = \frac{U_0}{I_0} \cdot e^{j\varphi} \tag{10}$$

where $j = \sqrt{-1}$ is the imaginary unit. The impedance can also be expressed in the form of a complex number, as the sum of a real component, $Re(Z)$, and an imaginary component, $Im(Z)$:

$$Z = Re(Z) + j \cdot Im(Z) \tag{11}$$

$Re(Z)$ represents the resistance of the system and $Im(Z)$ the reactance. Impedance spectra is usually represented graphically in the form of Nyquist plots, where the negative imaginary part of the impedance, $-Im(Z)$, is plotted over its real part, $Re(Z)$.

2.5. Measurement of conductivity as function of pH

The conductivity as a function of pH for H_3Cit/Na_3Cit and H_2Ox/Na_2Ox systems was determined by means of titration. Their respective salts were prepared at a concentration of 0.05 M. The corresponding acid was prepared at the same concentration, in order to ensure constant concentration of anions. 100 mL of the salt solution were stirred at room temperature (21 °C) and two electrodes were placed inside the solution to measure pH and conductivity. Subsequently, acid solution was poured in small volume steps, while pH and conductivity were registered.

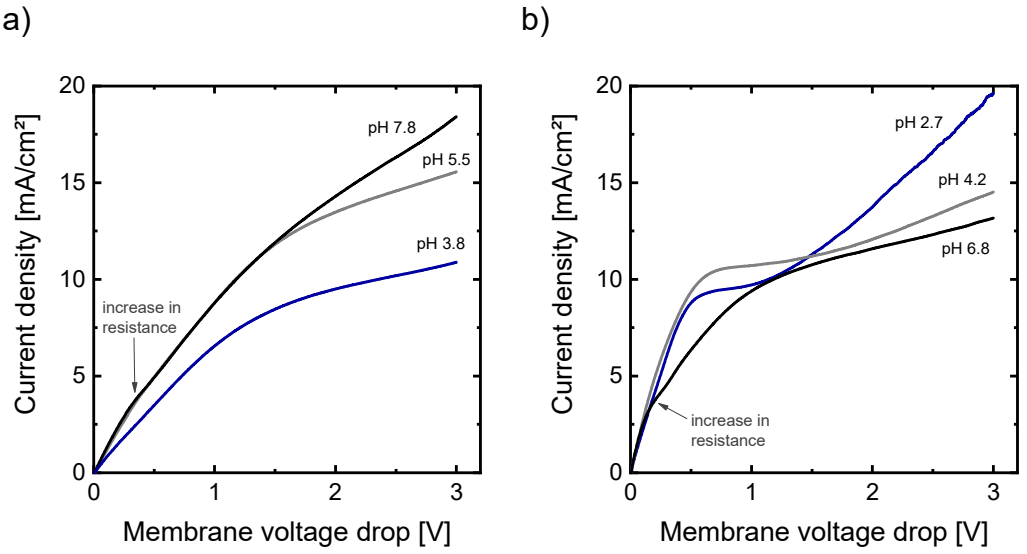

Figure 2: Current-voltage curves registered at different values of pH for (a) 0.05M H_3Cit/Na_3Cit solutions and (b) 0.05M H_2Ox/Na_2Ox solutions.

3. Results

3.1. Current-voltage characteristics

Current-voltage measurements conducted by linear sweep voltammetry for the two electrolyte systems, H_3Cit/Na_3Cit and H_2Ox/Na_2Ox, at different pH values are presented in Fig. 2. From the plots, it is evident that solution pH has a strong influence on the shape of the curves. For both systems, the curves obtained at acidic pH show the three characteristic regions typically obtained with strong electrolytes. First, at very low current densities, the current-voltage relationship is well described by a quasi-ohmic dependence, since membrane voltage drop increases linearly with current density. As the level of polarization is increased, depletion of ions at the diluting diffusion boundary layer involves a decrease in the concentration of ions from the bulk solution up to the membrane-solution interface. This decrease in concen-

tration is evidenced in the current-voltage curves in the form of a plateau region, thus reflecting the increased resistance of the system. The current density that marks the beginning of the plateau region, commonly termed as the limiting current density, i_{lim}, appears at about 7.5 mA/cm^2 for the H_3Cit/Na_3Cit solution having a pH of 3.8. In the case of the H_2Ox/Na_2Ox solutions at pH 2.7 and 4.2, the i_{lim} takes values around 8.5 and 9.5 mA/cm^2, respectively. The third region appearing at high current densities is characterized by an increase in the slope as a consequence of an enhanced supply of ions to the membrane depleting interface. As indicated in the introduction, overlimiting mass transfer phenomena include the dissociation of water and the onset of electroconvective vortices that produce mixing in the diffusion boundary layer. The third region can be clearly seen for the H_2Ox/Na_2Ox system at a pH of 2.7. On the contrary, for the H_3Cit/Na_3Cit system, overlimiting regions are not clearly seen within the range of applied voltages.

The polarization curves registered for solutions at the highest pH values (pH of 5.5 and 7.8 in Fig. 2(a) and pH of 6.8 in Fig. 2(b)) display an atypical evolution. Similar to results reported in previous publications dealing with weak electrolytes, more than two bending points (two i_{lim}: i_{lim1} and i_{lim2}) can be detected [24, 26, 39]. After the initial region of quasi-ohmic behavior, a first increase in membrane resistance is observed. This phenomenon occurs at current density values around 3.5 mA/cm^2 for both systems. As the current density is further increased, a tilted plateau is registered until another bending of the curves takes place. From this point on, the curves exhibit a second plateau, significantly flatter than the previous one. Given the flat-

ness and length of the second plateaus formed at $i > i_{lim2}$, electroconvection seems to play a minimal role at the range of DC bias applied in the present work. If the curves obtained at high and low pH values are compared in this range of current densities, it is clear from the plots that the second plateau evolves almost parallel to the only plateau registered in acidic conditions. This fact indicates that in both cases the phenomenon causing the increased system resistance is the same: the depletion of ions near the membrane when $i > i_{lim2}$. On the contrary, the phenomenon responsible for the i_{lim1} remains unclear at this point.

To further investigate the progress of concentration polarization, especially at current densities between i_{lim1} and i_{lim2}, chronopotentiometric measurements were carried out for each system. The chronopotentiograms are representations of the timely evolution of the membrane voltage drop, at constant current conditions, until a steady state is reached. Fig. 3 shows the correlation between the chronopotentiometric and the LSV measurements for 0.05 M Na_3Cit solutions. The chronopotentiograms show the typical profile reported for strong electrolytes: at low current densities (e.g. 3 mA/cm^2), only the quasi-ohmic resistance of the system is visible and the curves exhibit a flat response; as the i_{lim1} is reached, a sharp increase in voltage illustrates the development of concentration polarization. The last values of membrane voltage drop of the chronopotentiograms are representative for the steady state of the system. Thus, they can be represented against the corresponding current density to obtain the polarization curves. As can be seen in Fig. 3 (b), these representations are equivalent to the measurements con-

ducted by LSV. Fig. 4 shows the correlation between the polarization curves obtained by chronopotentiometry and LSV for Na_2Ox, where the match between both techniques is also corroborated. In addition to this, the absence of oscillations in the chronopotentiograms obtained at the highest current densities is also noticeable in both systems. The presence of oscillations in membrane voltage at overlimiting current densities has been generally associated with the development of electroconvective vortices at the diluate membrane side [39]. Thus, it can be inferred that electroconvection plays a minor role at the DC bias and with the membrane-electrolyte systems investigated in our study.

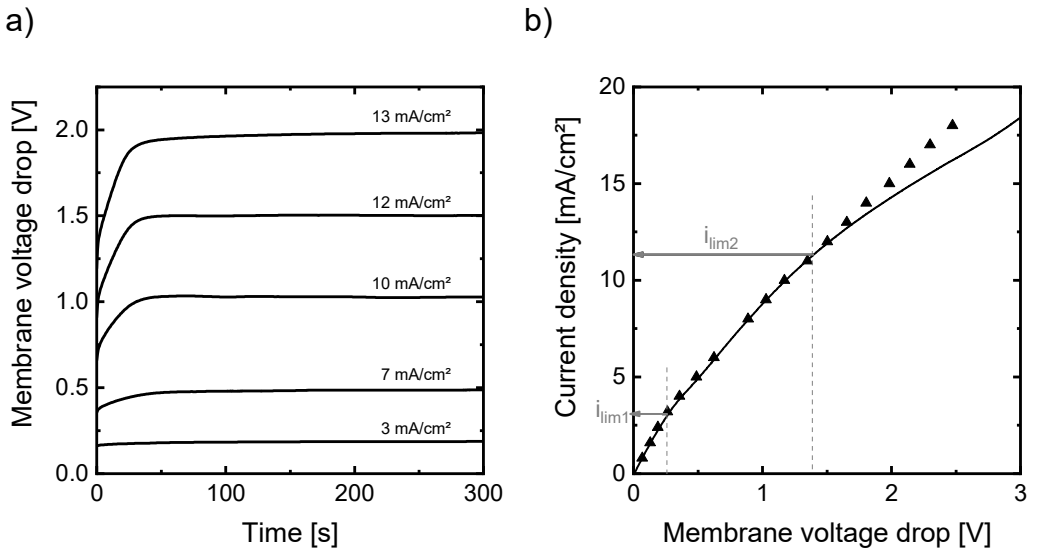

Figure 3: Comparison between the registered (a) chronopotentiograms and (b) the current-voltage curves for the 0.05M Na_3Cit solutions having a pH value of 7.8.

Despite the agreement between chronopotentiometry and LSV, no unequivocal information about the phenomenon responsible for the increased

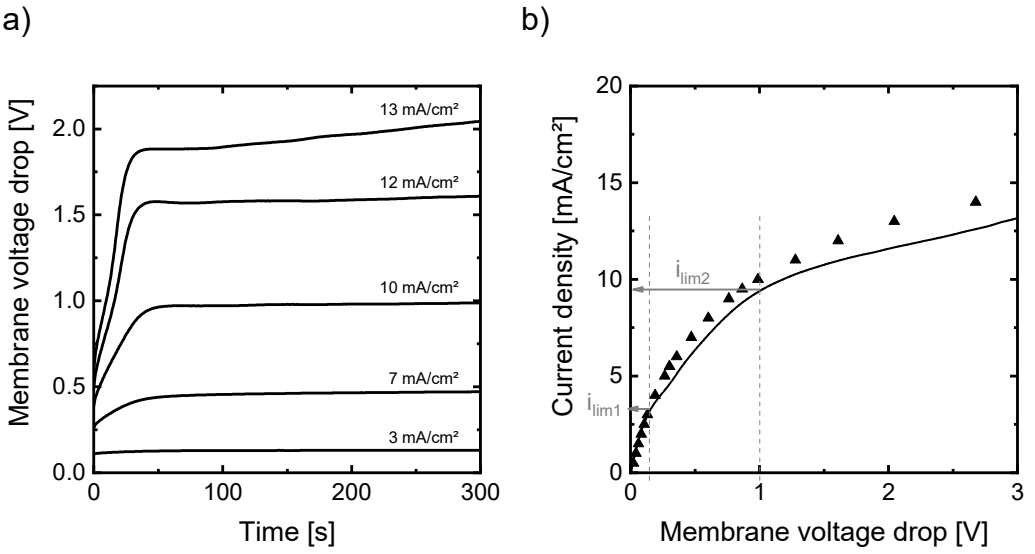

Figure 4: Comparison between the registered (a) chronopotentiograms and (b) the current-voltage curves for the 0.05M Na_2Ox solutions having a pH value of 6.8.

system resistance at currents between i_{lim1} and i_{lim2} can be extracted from the chronopotentiograms. This differs from previous studies, where useful information on different mass transfer processes could be obtained by means of chronopotentiometry [25, 40]. This fact reveals that the timescale at which such phenomenon takes place is probably shorter than the resolution of the measuring time. Hence, supportive information gathered from more powerful techniques which allow it to accurately access to phenomena that undergo at different rates is needed. To tackle this challenge, in the following section, EIS measurements will be analyzed for the elucidation of the physical phenomena that are behind the particular features observed during ED of organic acids.

3.2. Electrochemical impedance spectroscopy measurements at different current regimes

Electrochemical impedance measurements were conducted at different levels of potential bias, which were selected to fall within the characteristic regions of the polarization curves. EIS is based on the measurement of the relationship between the sinusoidal voltage and current signals registered between two points of a system at a wide range of frequencies. One of the main potentials of EIS is the identification of distinct mass transfer phenomena that are included in the global DC response of the system, but develop at different characteristic frequencies upon application of AC signals.

More specifically, the rates of ion transport across an electrochemical cell may differ based on the dielectric and conducting properties of each slab of the system. Previous experimental works on the impedance response of ion-exchange membranes typically showcase two main contributions to ion transport, which are described by two distinctive arcs in Nyquist diagrams [41–43]:

- A geometric arc appearing at the left side of the plots (high frequencies), which is associated with the ohmic conductivity of membrane and electrolyte.
- A diffusion arc appearing at the right side of the plots (low frequencies). This arc follows a 45° slope at medium frequencies and evolves into a semicircle as frequency tends to zero.

Depending on factors, such as the flow regime, the ion concentration or the

polarization level, each contribution may change its significance in relation to the overall system impedance. First, we show in Fig. 5 an exemplary representation of the effect of current density on the shape of complex-plane Nyquist plots for a strong electrolyte. NaCl systems are well-characterized in the literature and can serve as a reference to identify peculiarities in the spectra registered with organic acids. Impedance spectra corresponding to three characteristic points of the polarization curve are shown: (i) the quasi-ohmic region (lower-right panel), (ii) the plateau region (middle-right panel) and (iii) the overlimiting region (upper-right panel).

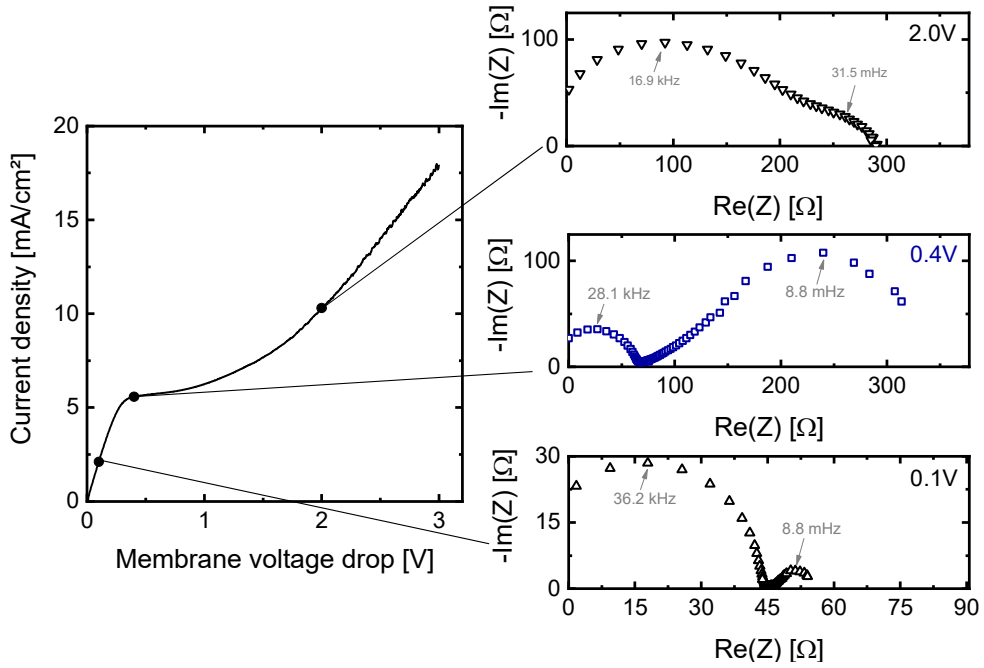

Figure 5: Current-voltage curve and EIS spectra obtained at different current regimes for 0.05 M NaCl solutions and the HDX200 membrane.

In the plot corresponding to the quasi-ohmic region, the geometric semi-

circle accounts for the major part of the system resistance, whereas the Warburg-type diffusion impedance is significantly smaller. These results are consistent with the low level of polarization achieved at 0.1 V, where the concentration profiles in the diffusion boundary layers are not fully developed. In this regime, diffusive limitations are not important yet, so that the main resistance to ion transport is associated with the migration of ions. An important parameter that can be obtained from each semicircle is the characteristic frequency. As indicated in the plots, the characteristic frequency corresponds to the measuring point at which the maximum of a semicircle is registered (i.e. the maximum in $-Im(Z)$). The inverse of this frequency represents the time constant of the process that is tracked by the semicircle in question. Time constants indicate how fast processes involved during ion transport occur until a new steady state of the membrane system is attained. The Nyquist plot obtained at DC bias of 0.1 V has two characteristic frequencies, 36.2 kHz for the geometric and 8.8 mHz for the Warburg arc, thus reflecting that diffusive processes develop significantly slower than ion migration.

When the DC bias is increased beyond the i_{lim}, the diameter of the Warburg semicircle grows substantially, becoming the predominant resistance in the system. Here, it is to note that the scale of the graph has been adapted to properly show the total system resistance. In the plateau region after surpassing the i_{lim}, concentration profiles should have been fully developed. Accordingly, the concentration of ions at the diluate membrane/solution interface tends to zero, so that the main resistance to ion transport is located

in this part of the system.

The spectrum obtained at DC bias corresponding to the region of overlimiting current densities displays two overlapping arcs. According to the shape of the current-voltage curves, the current density rises again with the membrane voltage drop, which implies that the supply of anions to the membrane surface has been triggered. It is also noteworthy, that the overall membrane resistance, which can be extracted from the intercept with the x-axis at very low frequencies, is lower than the resistance obtained at DC of 0.4 V (plateau region). The characteristic frequency of the second arc is close to 31.5 mHz, notably differing from the frequencies associated with a Warburg-type impedance. Thus, the catalytic dissociation of waterand the transport of OH^- ions through the membrane seems to be the reason for the reduction in resistance and the presence of the second arc. The dissociation of water in anion-exchange membranes at overlimiting currents has been studied via EIS by Kniaginichieva et al [44]. It was found that all arcs of Nyquist plots merge at current densities higher than $1.5 \cdot i_{lim}$. The results shown in the upper-right panel of Fig. 5 follow this trend. In this case, the current transfer across the membrane is carried by the product ions of water dissociation, so that the diffusion limitation is not apparent in the plots as it was for lower DC bias.

Following with the impedance spectra obtained with organic acids at different current density regimes, Fig. 6 shows the Nyquist plots obtained for Na_3Cit solutions. At very low polarization levels ($i < i_{lim1}$), the spectrum

obtained is analogous to those previously described for strong electrolytes. Both the geometric and diffusive arcs become evident and are well separated from each other in the plots. Furthermore, the characteristic frequencies correspond to the same range of frequencies that are distinctive of migration- and diffusion-limited mass transfer processes.

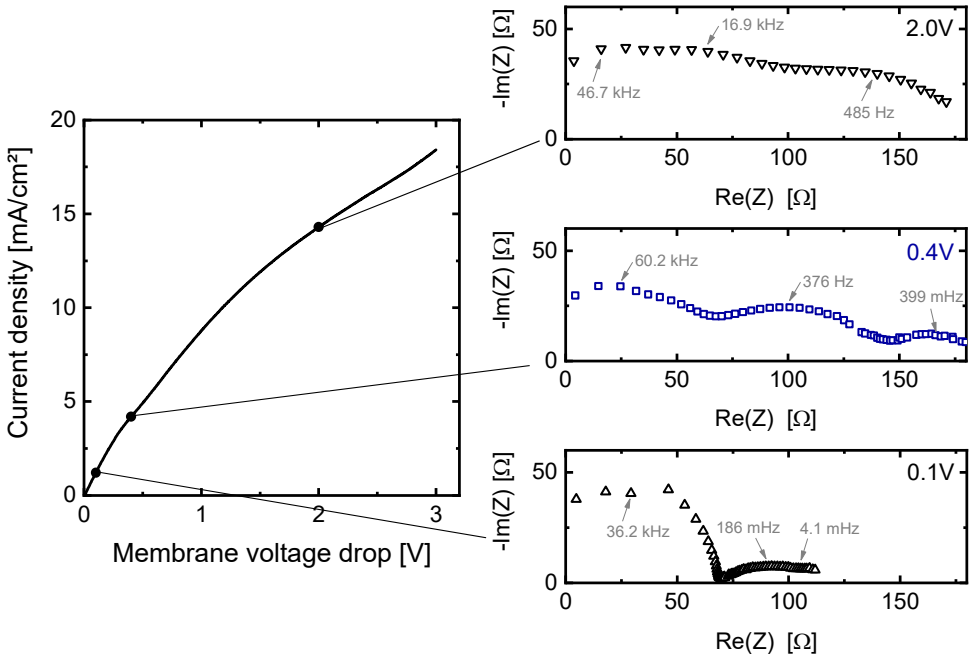

Figure 6: Current-voltage curve and EIS spectra obtained at different current regimes for 0.05 M Na_3Cit solutions with a pH of 7.8.

When the background DC bias is slightly increased up to 0.4 V and the first tilted plateau is reached (characteristic of organic acids at high pH values, i.e. $i_{lim1} < i < i_{lim2}$), the shape of the impedance spectrum undergoes notorious changes. The plots contain interesting features not observed with strong electrolytes. In this case, the spectrum presents three different

semicircles, which are slightly overlapped with each other. While the arc appearing in the left has a characteristic frequency in the same order of magnitude as the geometric arcs observed at lower DC voltages, the characteristic frequencies of the second and third arc do not belong to the timescales of diffusion-controlled processes. Moreover, the phenomena associated with the emergence of the two additional arcs at medium frequencies causes an increase in the overall system resistance.

A further increase in DC bias to fall in the second plateau region ($i > i_{lim2}$) results in impedance spectra with similar shape as in the second plateau region. The three different arcs can be hardly identified because the overlapping between them becomes stronger. In this case, the maxima of the second and third arc are displaced toward higher frequencies. The characteristic frequency changes from 376 Hz to 16.9 kHz for the middle arc and from 399 mHz to 485 Hz for the third arc, when increasing the DC bias level from 0.4 to 2 V. The shifts indicate that the processes associated with the middle-frequency arcs speed up with an increase in the polarization level.

The impedance spectra obtained with Na_2Ox solutions are shown in Fig. 7. In this case, Nyquist plots evolve similarly as for Na_3Cit solutions, where additional arcs appear at increasing DC bias, and then, at the highest applied voltages, all arcs merge into a distorted semicircle. It has to be noted that the arcs appearing at intermediate frequencies may be more or less evident based on the different equilibrium reactions taking place in each system. In this sense, H_3Cit is a tricarboxylic acid and can generate mixtures

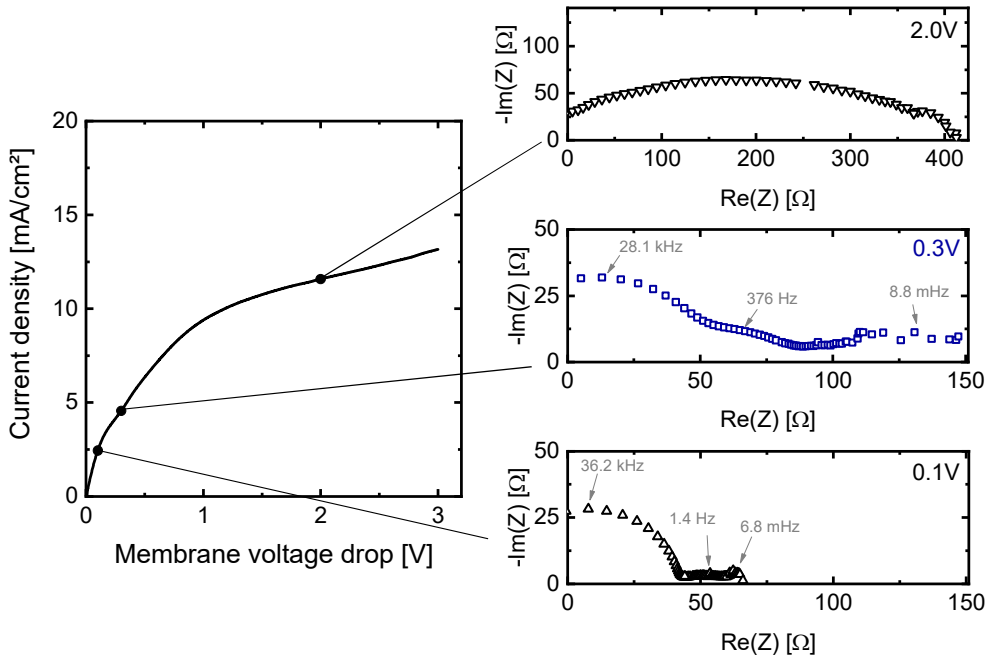

Figure 7: Current-voltage curve and EIS spectra obtained at different current regimes for 0.05 M Na_2Ox solutions with a pH of 6.8.

with a higher number of species, as compared with H_2Ox.

In contrast with the EIS results registered for strong electrolytes, the arcs showing up at middle frequencies in Fig. 6 and Fig. 7 indicate that additional mass transfer phenomena take place during ED of organic acids. Such phenomena occur at characteristic frequencies significantly apart from each other and tend to merge into one arc as the polarization level is increased. Although the arcs becoming visible at increasing DC bias appear at the right side of the Nyquist plots, their characteristic frequencies indicate that the associated phenomena are not related to diffusion-limited mass transfer processes. In similar studies, the emergence of intermediate arcs at

increasing currents has been attributed to a Gerischer impedance associated with the progress of the catalyzed water dissociation reaction[44, 45]. The results obtained in our study point in the same direction, as revealed in Fig. 5 for NaCl solutions. However, pH could be only measured in the bulk solution, where changes smaller than 0.5 units of pH were obtained. Harding et al. also reported similar impedance spectra when investigating the dielectric response of rotating disc electrodes with coupled electrochemical and homogeneous reactions [46].

Nonetheless, our impedance results differ from previous works in the fact that, not only one additional arc evolves at intermediate frequencies, but at least, two additional arcs are registered. In this regard, OH^- and H^+ ions generated at the membrane-solution interfacedo not seem to be the only species transported through the membranes in the range of current densities between i_{lim1} and i_{lim2}. While OH^- ions may migrate through the membrane, the generated H^+ ions at the diluting membrane solution-interface may contribute to decrease the pH in the solution layer near the membrane. Experimental measurements showed that pH changes in the bulk are minimal, so that the solution layer where significant pH changes occur should be very thin. This hypothesis was also considered by Nikonenko et al. for modelling the transport of carbonic acid anions through anion-exchange membranes [47]. According to the speciation diagrams shown in Fig. 1, even a very small decrease in pH in a thin solution layer near the diluting membrane-solution interface would displace the equilibrium towards the formation of organic anions of lower charge. Simultaneously, the generation of H^+ and

445 OH^- ionswould concatenate additional homogeneous reactions. Thus, the
446 additional arcs showing up in the Nyquist plots at intermediate frequencies
447 correlate with chain homogeneous reactions triggered by the dissociation of
448 water mediated by the membrane fixed charges.

449

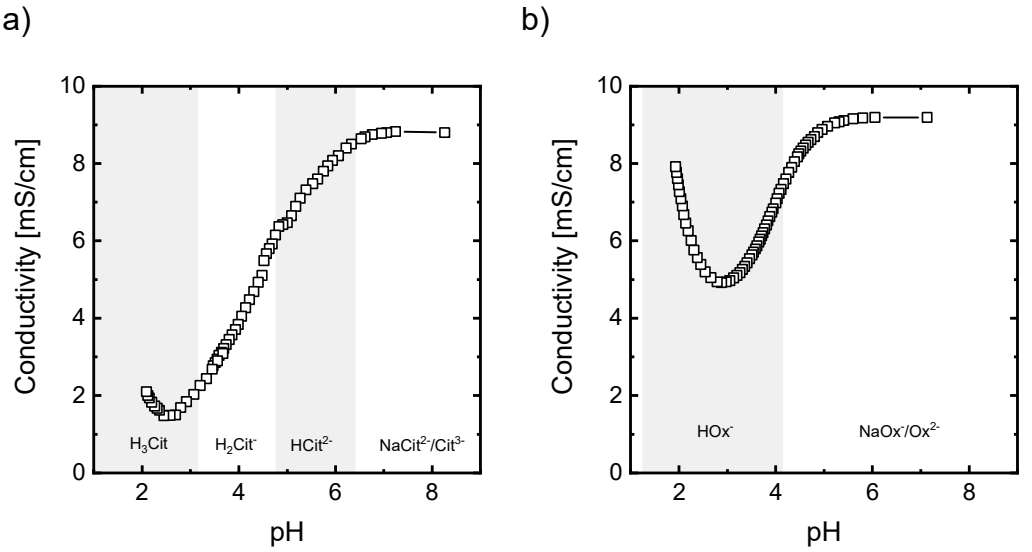

Figure 8: pH-conductivity titration curves obtained for a total anion concentration of 0.05M with the systems (a) H_3Cit/Na_3Cit and (b) H_2Ox/Na_2Ox . The figures show the relationship between solution pH and conductivity. Areas of different colors show the regions of predominance of different species.

450 The impedance results obtained for different DC bias with solutions of
451 H_2Ox and H_3Cit of lower pH values are analogous to those obtained for the
452 highest pH values at low polarization levels (corresponding to the lower-right
453 panel of Fig. 6 and Fig. 7). Thus, solutions of the organic acids at pH values
454 where the monovalent acid anions (i.e. HOx^- and H_2Cit^-) predominate in
455 the bulk solution also show a similar behavior as the one described above for
456 strong electrolytes. The absence of multiple Gerischer arcs can be explained

by the fact that monovalent acid anions can only undergo protonation reactions at very low pH values, giving rise to non-charged species. On the contrary, at high pH values, where multivalent anions are the main species in the bulk solution, the generation of a small number of H^+ ions already implies a change in the predominating species, thus altering the conductivity of the system.The influence of the charge of acid anions on the conductivity of the system can also be deduced from the relationship between solution conductivity and pH depicted in Fig. 8. The shadowed and white sectors represent the regions of predominance of the different species. Here, it is confirmed that for both systems, when starting from high pH values, the formation of monovalent anions at decreasing pH is accompanied by a decrease in conductivity. Furthermore, the decrease in conductivity is consistent with the concatenation of equilibrium reactions and the conversion of multivalent anions into monovalent ones. In other words, once water molecules are strongly polarized near the membrane fixed charges, the resulting H^+ ions migrate towards the cathode, finding on their way acid anions and displacing reactions (2), (3) or (6) towards the left. This correlation results especially evident for the H_2Ox/Na_2Ox system, since the minimum in conductivity at a pH of 2.7 coincides with the maximum proportion of HOx^- anions in the speciation diagrams of Fig. 1(b). Therefore, the change in ionic conductivity of the thin reaction layer near the membrane, along with the reaction impedance, add up to the intensification of concentration polarization and explain the formation of the tilted plateaus at current densities between i_{lim1} and i_{lim2}. The progressive depletion of acid species results in the subsequent bending of the polarization curves at i_{lim2}.

4. Conclusions

Transport of citric and oxalic acid solutions through anion-exchange membranes has been investigated via multiple electrochemical measurement techniques. Here, we have addressed the challenge of characterizing the main phenomena responsible for the atypical current-voltage behavior observed in such systems. Results have shown that EIS is a highly informative technique allowing it to probe relatively fast reactions triggered by the onset of catalytic

- Electrodialysis of organic acids conducted in the region of predominance of multiply charged anions is characterized by the registration of current-voltage curves with two i_{lim}. An increase in the system resistance at current densities between i_{lim1} and i_{lim2} is manifested in the form of a tilted plateau in the curves. Consequently, the first limiting current density cannot be ascribed to the complete exhaustion of ions near the membrane surface.

- The timely resolution of conventional dynamic techniques, such as chronopotentiometry, is not sufficient for elucidating the phenomenon causing the first plateau. In contrast, phenomena taking place within a wide spectrum of frequencies can be accessed via EIS, thus enabling the identification of multiple events of distinct nature contributing to the total system resistance.

- The progress of H^+ and OH^- ions generation, along with homogeneous protonation reactions of weak acid anions, are fingerprinted by multiple Gerischer arcs appearing at intermediate frequencies in Nyquist diagrams. The Gerischer arcs, i.e. homogeneous electrolyte rections,

induce an increase in the system resistance which is connected with the tilted plateaus of the current-voltage curves.

- Beyond the i_{lim1}, dissociation of water becomes progressively intensified with the polarization level. As a consequence, homogeneous reactions involving organic acid anions speed up. This phenomenon is tracked by a gradual increase in the Gerischer characteristic frequencies and, ultimately, by the merging at very high DC bias of several semicircles in the Nyquist plots.

The mass transfer phenomena characterized in the present work are common to the two investigated organic acids. Thus, with the basis set up in the present work, further research focusing on the investigation of other relevant system parameters, such as the membrane type, the total electrolyte concentration, or transport of more complex mixtures through ion-exchange membranes, is expected to result in optimum operating and monitoring strategies leading to high-efficient systems for the recovery of organic acids.

Acknowledgement

M.C. Martí-Calatayud acknowledges the support of Generalitat Valenciana through the funding APOSTD/2017/059.

References

[1] A. A. Kiss, J. P. Lange, B. Schuur, D. W. Brilman, A. G. van der Ham, S. R. Kersten, Separation technology–Making a difference in biorefineries, Biomass and Bioenergy 95 (2016) 296–309.

[2] C. Abels, F. Carstensen, M. Wessling, Membrane processes in biorefinery applications, Journal of Membrane Science 444 (2013) 285–317.

[3] Z. Sun, B. Fridrich, A. De Santi, S. Elangovan, K. Barta, Bright Side of Lignin Depolymerization: Toward New Platform Chemicals, Chemical Reviews 118 (2) (2018) 614–678.

[4] M. Wang, J. Ma, H. Liu, N. Luo, Z. Zhao, F. Wang, Sustainable Productions of Organic Acids and Their Derivatives from Biomass via Selective Oxidative Cleavage of C-C Bond, ACS Catalysis 8 (3) (2018) 2129–2165.

[5] A. A. Koutinas, A. Vlysidis, D. Pleissner, N. Kopsahelis, I. Lopez Garcia, I. K. Kookos, S. Papanikolaou, T. H. Kwan, C. S. K. Lin, Valorization of industrial waste and by-product streams via fermentation for the production of chemicals and biopolymers, Chemical Society Reviews 43 (8) (2014) 2587.

[6] E. Betiku, H. A. Emeko, B. O. Solomon, Fermentation parameter optimization of microbial oxalic acid production from cashew apple juice, Heliyon 2 (2016) e00082.

[7] L. Regestein, T. Klement, P. Grande, D. Kreyenschulte, B. Heyman, T. Maßmann, A. Eggert, R. Sengpiel, Y. Wang, N. Wierckx, L. M. Blank, A. Spiess, W. Leitner, C. Bolm, M. Wessling, A. Jupke, M. Rosenbaum, J. Büchs, From beech wood to itaconic acid: Case study on biorefinery process integration, Biotechnology for Biofuels 11 (1) (2018) 1–11.

[8] D. Di Marino, T. Jestel, C. Marks, J. Viell, M. Blindert, S. M. Kriescher, A. C. Spiess, M. Wessling, Carboxylic Acids Production via Electrochemical Depolymerization of Lignin, ChemElectroChem 6 (5) (2019) 1434–1442.

[9] C. S. López-Garzón, A. J. J. Straathof, Recovery of carboxylic acids produced by fermentation, Biotechnology Advances 32 (5) (2014) 873–904.

[10] L. Handojo, A. K. Wardani, D. Regina, C. Bella, M. T. Kresnowati, I. G. Wenten, Electro-membrane processes for organic acid recovery, RSC Advances 9 (14) (2019) 7854–7869.

[11] C. Jiang, Y. Wang, T. Xu, Membranes for the recovery of organic acids from fermentation broths, in: A. Figoli, A. Cassano, A. Basile (Eds.), Membrane Technologies for Biorefining, Woodhead Publishing, Duxford (UK), 2016, pp. 135–161.

[12] J. Stodollick, R. Femmer, M. Gloede, T. Melin, M. Wessling, Electrodialysis of itaconic acid: A short-cut model quantifying the electrical resistance in the overlimiting current density region, Journal of Membrane Science 453 (2014) 275–281.

[13] E. Brauns, Towards a worldwide sustainable and simultaneous large-scale production of renewable energy and potable water through salinity gradient power by combining reversed electrodialysis and solar power?, Desalination 219 (1-3) (2008) 312–323.

[14] S. Abu Khalla, M. Suss, Desalination via chemical energy: An electrodialysis cell driven by spontaneous electrode reactions, Desalination 467 (April) (2019) 257–262.

[15] A. Chandra, J. G. D. Tadimeti, S. Chattopadhyay, Transport hindrances with electrodialytic recovery of citric acid from solution of strong electrolytes, Chinese Journal of Chemical Engineering 26 (2) (2018) 278–292.

[16] S. J. Andersen, T. Hennebel, S. Gildemyn, M. Coma, J. Desloover, J. Berton, J. Tsukamoto, C. Stevens, K. Rabaey, Electrolytic Membrane Extraction Enables Production of Fine Chemicals from Biorefinery Sidestreams, Environmental science & technology 48 (2014) 7135–7142.

[17] R. J. Jones, J. Massanet-Nicolau, A. Guwy, G. C. Premier, R. M. Dinsdale, M. Reilly, Removal and recovery of inhibitory volatile fatty acids from mixed acid fermentations by conventional electrodialysis, Bioresource Technology 189 (2015) 279–284.

[18] P. Chai, J. Wang, H. Lu, The cleaner production of monosodium l-glutamate by resin-filled electro-membrane reactor, Journal of Membrane Science 493 (2015) 549–556.

[19] L. Fu, X. Gao, Y. Yang, F. Aiyong, H. Hao, C. Gao, Preparation of succinic acid using bipolar membrane electrodialysis, Separation and Purification Technology 127 (2014) 212–218.

[20] M. Kumar, B. P. Tripathi, V. K. Shahi, Electro-membrane reactor for separation and in situ ion substitution of glutamic acid from its sodium salt, Electrochimica Acta 54 (21) (2009) 4880–4887.

[21] N. Pismenskaya, V. Nikonenko, B. Auclair, G. Pourcelly, Transport of weak-electrolyte anions through anion exchange membranes, Journal of Membrane Science 189 (1) (2001) 129–140.

[22] M. Martí-Calatayud, D. C. Buzzi, M. García-Gabaldón, E. Ortega, A. M. Bernardes, J. A. S. Tenório, V. Pérez-Herranz, Sulfuric acid recovery from acid mine drainage by means of electrodialysis, Desalination 343 (2014) 120–127.

[23] M. C. Martí-Calatayud, D. C. Buzzi, M. García-Gabaldón, A. M. Bernardes, J. A. S. Tenório, V. Pérez-Herranz, Ion transport through homogeneous and heterogeneous ion-exchange membranes in single salt and multicomponent electrolyte solutions, Journal of Membrane Science 466 (2014) 45–57.

[24] E. D. Belashova, N. D. Pismenskaya, V. V. Nikonenko, P. Sistat, G. Pourcelly, Current-voltage characteristic of anion-exchange membrane in monosodium phosphate solution. Modelling and experiment, Journal of Membrane Science 542 (2017) 177–185.

[25] M. C. Martí-Calatayud, M. García-Gabaldón, V. Pérez-Herranz, Mass Transfer Phenomena during Electrodialysis of Multivalent Ions: Chemical Equilibria and Overlimiting Currents, Applied Sciences 8 (9) (2018) 1566.

[26] E. D. Melnikova, N. D. Pismenskaya, L. Bazinet, S. Mikhaylin, V. V. Nikonenko, Effect of ampholyte nature on current-voltage characteristic of anion-exchange membrane, Electrochimica Acta 285 (2018) 185–191.

[27] O. Rybalkina, K. Tsygurina, E. Melnikova, S. Mareev, I. Moroz, Partial Fluxes of Phosphoric Acid Anions through Anion-Exchange Membranes in the Course of NaH 2 PO 4 Solution Electrodialysis, International Journal of Molecular Sciences 20 (3593) (2019) 1–22.

[28] R. Femmer, A. Mani, M. Wessling, Ion transport through electrolyte/polyelectrolyte multi-layers, Scientific Reports 5 (2015) 11583.

[29] T. Belloň, P. Polezhaev, L. Vobecká, M. Svoboda, Z. Slouka, Experimental observation of phenomena developing on ion-exchange systems during current-voltage curve measurement, Journal of Membrane Science 572 (November 2018) (2019) 607–618.

[30] O. A. Rybalkina, K. A. Tsygurina, E. D. Melnikova, G. Pourcelly, V. V. Nikonenko, N. D. Pismenskaya, Catalytic effect of ammonia-containing species on water splitting during electrodialysis with ion-exchange membranes, Electrochimica Acta 299 (2019) 946–962.

[31] Y. Tanaka, Water dissociation reaction generated in an ion exchange membrane, Journal of Membrane Science 350 (1-2) (2010) 347–360.

[32] E. I. Belova, G. Y. Lopatkova, N. D. Pismenskaya, V. V. Nikonenko, C. Larchet, G. Pourcelly, Effect of anion-exchange membrane surface properties on mechanisms of overlimiting mass transfer, Journal of Physical Chemistry B 110 (27) (2006) 13458–13469.

[33] E. Belova, G. Lopatkova, N. Pismenskaya, V. Nikonenko, C. Larchet, Role of water splitting in development of electroconvection in ion-exchange membrane systems, Desalination 199 (1-3) (2006) 59–61.

[34] V. I. Zabolotskiy, A. Y. But, V. I. Vasil'eva, E. M. Akberova, S. S. Melnikov, Ion transport and electrochemical stability of strongly basic anion-exchange membranes under high current electrodialysis conditions, Journal of Membrane Science 526 (November 2016) (2017) 60–72.

[35] D. Harvey, Modern analytical chemistry, mcgraw-hill Edition, McGraw-Hill, Boston, 2000.

[36] M. Papagianni, Advances in citric acid fermentation by Aspergillus niger: Biochemical aspects, membrane transport and modeling, Biotechnology Advances 25 (3) (2007) 244–263.

[37] P. Komáromy, P. Bakonyi, A. Kucska, G. Tóth, L. Gubicza, K. Bélafi-Bakó, N. Nemestóthy, Optimized pH and Its Control Strategy Lead to Enhanced Itaconic Acid Fermentation by Aspergillus terreus on Glucose Substrate, Fermentation 5 (2) (2019) 31.

[38] M. C. Martí-Calatayud, M. García-Gabaldón, V. Pérez-Herranz, Study of the effects of the applied current regime and the concentration of chromic acid on the transport of Ni^{2+} ions through Nafion 117 membranes, Journal of Membrane Science 392-393 (2012) 137–149.

[39] M. C. Martí-Calatayud, M. García-Gabaldón, V. Pérez-Herranz, Effect of the equilibria of multivalent metal sulfates on the transport

through cation-exchange membranes at different current regimes, Journal of Membrane Science 443 (2013) 181–192.

[40] D. Y. Butylskii, S. A. Mareev, N. D. Pismenskaya, P. Y. Apel, O. A. Polezhaeva, V. V. Nikonenko, Phenomenon of two transition times in chronopotentiometry of electrically inhomogeneous ion exchange membranes, Electrochimica Acta 273 (2018) 289–299.

[41] A. A. Moya, Electrochemical Impedance of Ion-Exchange Membranes with Interfacial Charge Transfer Resistances, The Journal of Physical Chemistry C (2016) acs.jpcc.5b12087.

[42] R. Femmer, M. C. Martí-Calatayud, M. Wessling, Mechanistic modeling of the dielectric impedance of layered membrane architectures, Journal of Membrane Science 520 (2016) 29–36.

[43] F. Roghmans, M. C. Martí-Calatayud, S. Abdu, R. Femmer, R. Tiwari, A. Walther, M. Wessling, Electrochemical impedance spectroscopy fingerprints the ion selectivity of microgel functionalized ion-exchange membranes, Electrochemistry Communications 72 (2016) 113–117.

[44] E. Kniaginicheva, N. Pismenskaya, S. Melnikov, E. Belashova, P. Sistat, M. Cretin, V. Nikonenko, Water splitting at an anion-exchange membrane as studied by impedance spectroscopy, Journal of Membrane Science 496 (2015) 78–83.

[45] N. D. Pismenskaya, E. V. Pokhidnia, G. Pourcelly, V. V. Nikonenko, Can the electrochemical performance of heterogeneous ion-exchange mem-

branes be better than that of homogeneous membranes?, Journal of Membrane Science 566 (June) (2018) 54–68.

[46] M. S. Harding, B. Tribollet, V. Vivier, M. E. Orazem, The Influence of Homogeneous Reactions on the Impedance Response of a Rotating Disk Electrode, Journal of The Electrochemical Society 164 (11) (2017) E3418–E3428.

[47] V. Nikonenko, K. Lebedev, J. A. Manzanares, G. Pourcelly, Modelling the transport of carbonic acid anions through anion-exchange membranes, Electrochimica Acta 48 (24) (2003) 3639–3650.